Supporting Information

Chimie Douce Derived Novel P2-type Layered Oxide for Potassium-Ion Batteries

*Pawan Kumar Jha, Alexander Golubnichiy, Dorothy Sachdeva, Abhik Banerjee, Gopalakrishnan Sai Gautam, Artem M. Abakumov, Maximilian Fichtner, and Prabeer Barpanda**

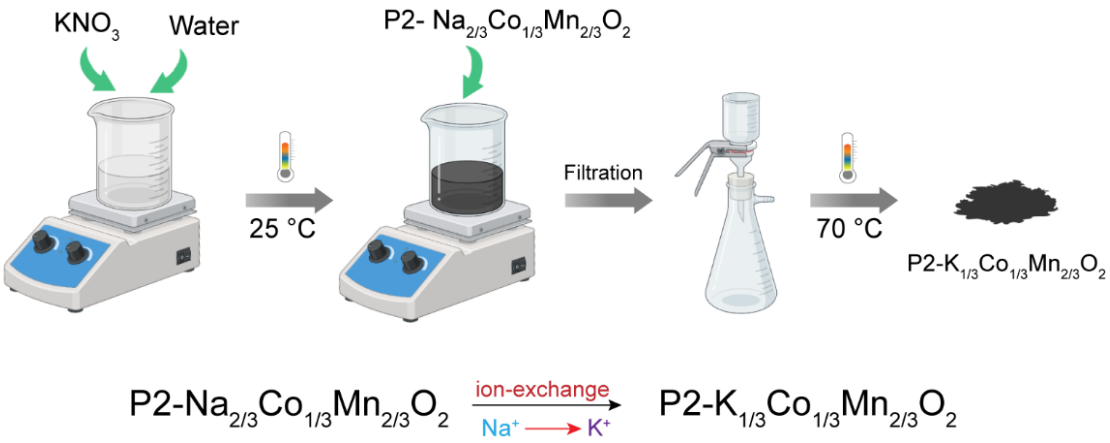

Figure S1. Schematic of steps followed in the soft chemistry-based ion exchange process.

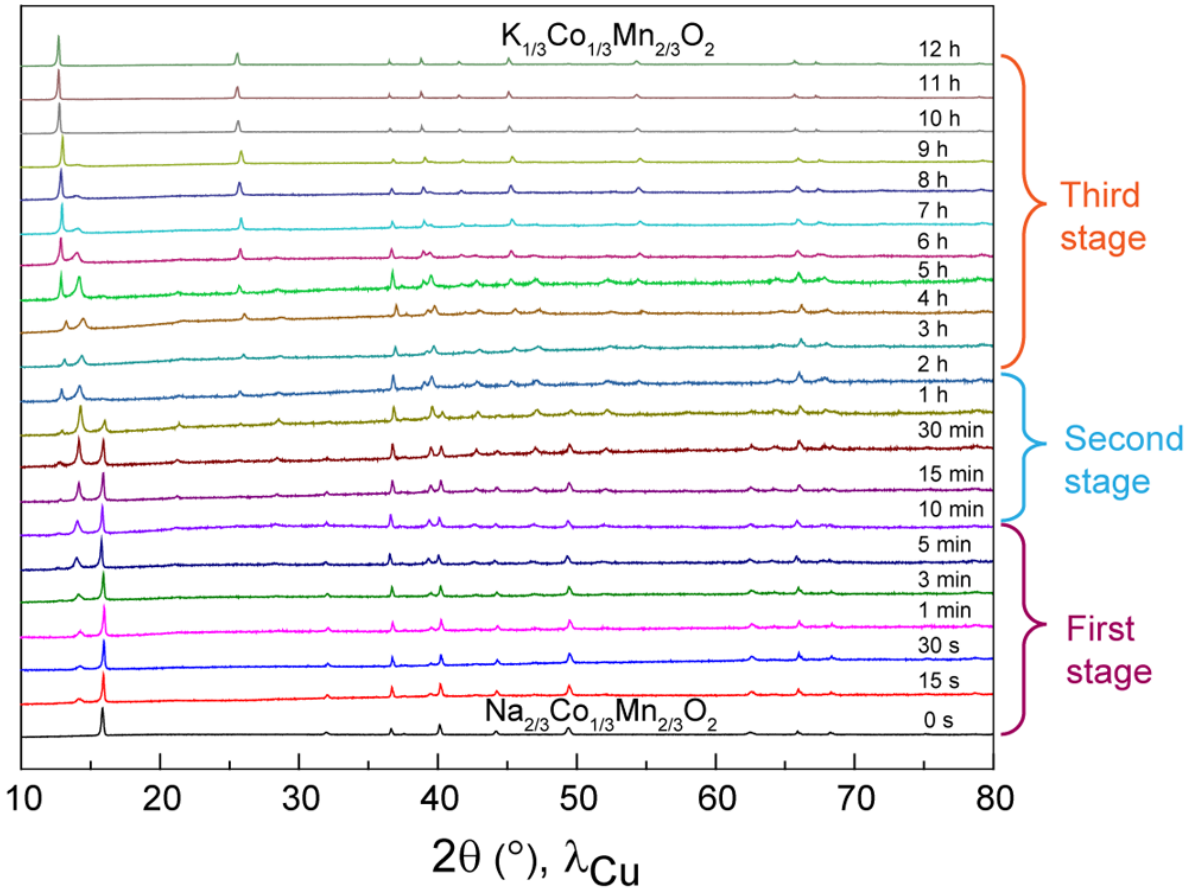

Figure S2. Ex situ X-ray powder diffraction (XRD) patterns of $K_xNa_{1-x}Co_{1/3}Mn_{2/3}O_2$ at room temperature, illustrating the dynamic evolution during the *chimie douce* reaction. It captures the changes in the material's structure as the reaction progresses in three stages.

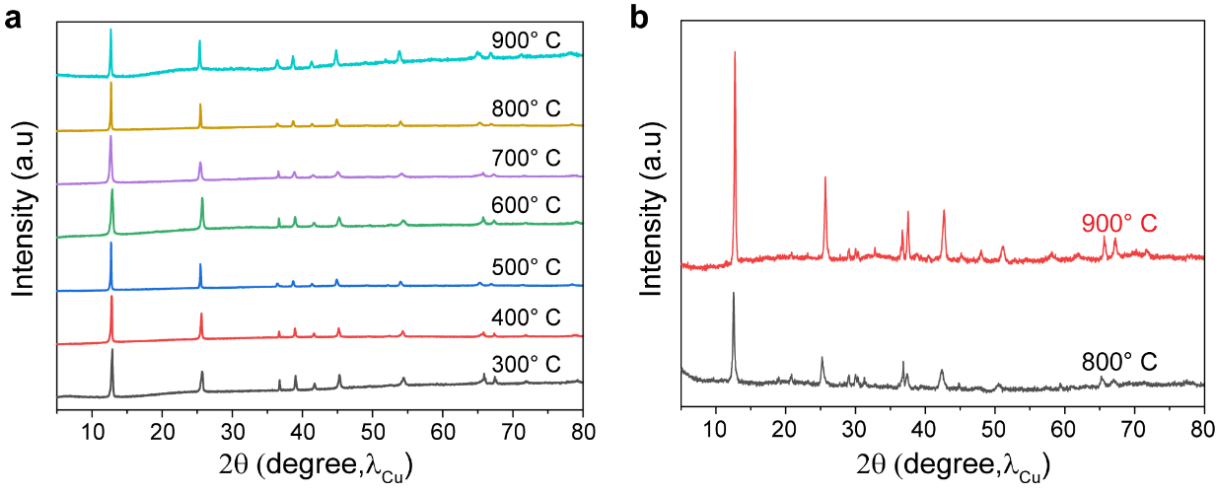

Figure S3. (a) Comparative XRD patterns at elevated temperature showing the thermal stability of P2-type $K_{1/3}Co_{1/3}Mn_{2/3}O_2$ product obtained by soft chemistry ion-exchange route. (b) XRD patterns of products formed by solid state reaction at 800° and 900°C for 12 h.They form P3-type phases along with other impurities.

Table S1. Crystallographic parameters of the parent P2-type $Na_{2/3}Co_{1/3}Mn_{2/3}O_2$ phase as derived from Rietveld refinement of laboratory XRD pattern (λ = 1.5405 Å).

Formula (molecular weight)	**$Na_{2/3}Co_{1/3}Mn_{2/3}O_2$ (107.65 g/mol)**
Crystal system	Hexagonal
Space group	*P*6$_3$/*mmc* (#194)
Unit cell parameter (Å)	*a* = 2.833551(2) *c* = 11.209989(7) *Z* = 2
Unit cell volume (Å^3)	77.9467(2)
Theoretical density (g cm^{-3})	4.58
Goodness of fit value	R_F= 9.615%, Bragg R-factor= 7.785%, χ^2 = 8.41%

Atom	Site	x	y	z	Occupancy
Co1	2*a*	0.0000	0.0000	0.0000	0.3273(9)
Mn1	2*a*	0.0000	0.0000	0.0000	0.6625(8)
Na1	2*b*	0.0000	0.0000	0.2500	0.2838(5)
Na2	2*d*	0.6667	0.3333	0.2500	0.405(2)
O1	4*f*	0.33330	0.6667	0.0968(6)	1.000

Table S2. Crystallographic parameters of the P2-type $K_{1/3}Co_{1/3}Mn_{2/3}O_2$ product phase derived from Rietveld refinement of synchrotron XRD pattern (λ = 1.033202 Å).

Formula (molecular weight)	**$K_{1/3}Co_{1/3}Mn_{2/3}O_2$ (101.28 g/mol)**
Crystal system	Hexagonal
Space group	*P*6$_3$/*mmc* (#194)
Unit cell parameter (Å)	*a* = 2.842646(1) *c* = 13.957900(1) *Z* = 2
Unit cell volume (Å^3)	97.6167(7)
Theoretical density (g cm^{-3})	3.44
Goodness of fit value	R_F= 7.048%, Bragg R-factor = 8.399%, χ^2 = 3.42

Atom	Site	x	y	z	Occupancy
Co1	2*a*	0.0000	0.0000	0.0000	0.339(9)
Mn1	2*a*	0.0000	0.0000	0.0000	0.675(5)
K1	2*b*	0.0000	0.0000	0.2500	0.115(6)
K2	2*d*	0.6667	0.3333	0.2500	0.226(7)
O1	4*f*	0.33330	0.6667	0.0675(9)	1.000

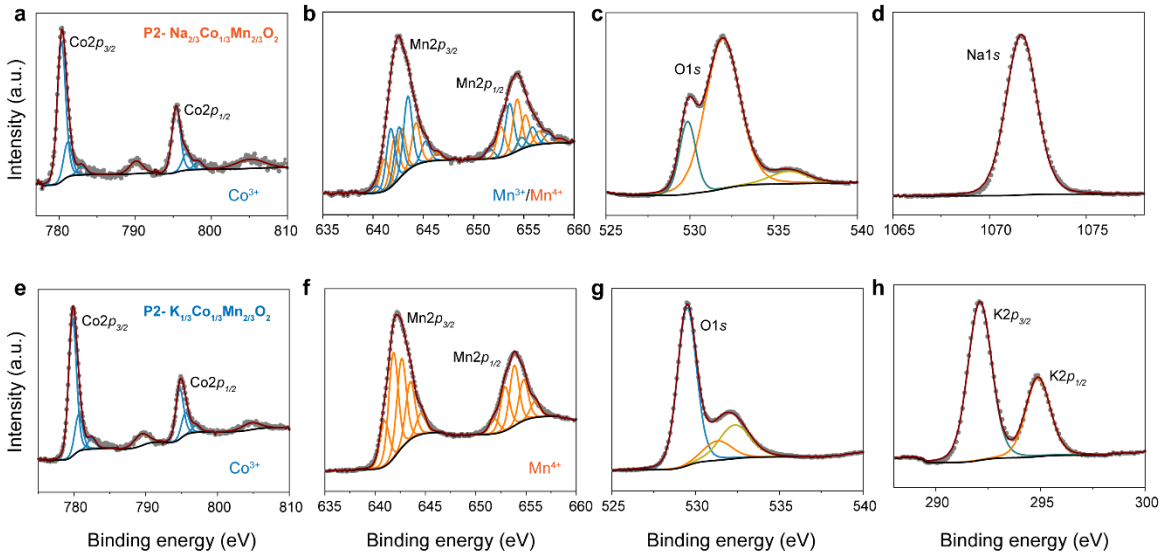

Figure S4. XPS spectra for constituent elements in (a-d) initial NCM and (e-h) final KCM phase. The blue curves and orange curves in Mn 2*p* spectra correspond to 3+ and +4 oxidation states.

Table S3. XPS analysis of the initial NCM and final KCM phases. Binding energies are given in eV.

Mn		NCM	KCM
Mn-2$p_{3/2}$ (f.w.h.m-1 eV)	4+	641.13	640.92
		642.16	641.81
		642.82	642.63
		644.27	643.49
		646.41	644.57
Mn-2$p_{3/2}$ (f.w.h.m-1 eV)	3+	640.31	--
		641.76	
		642.57	
		643.46	
		645.23	

Co		NCM	KCM
Co-2$p_{3/2}$ (eV)	3+	780.32	779.80
		781.15	780.67
		782.99	782.48
		790.13 ^{sat} (f.w.h.m-2.01 eV)	789.54 ^{sat} (f.w.h.m-2.21 eV)

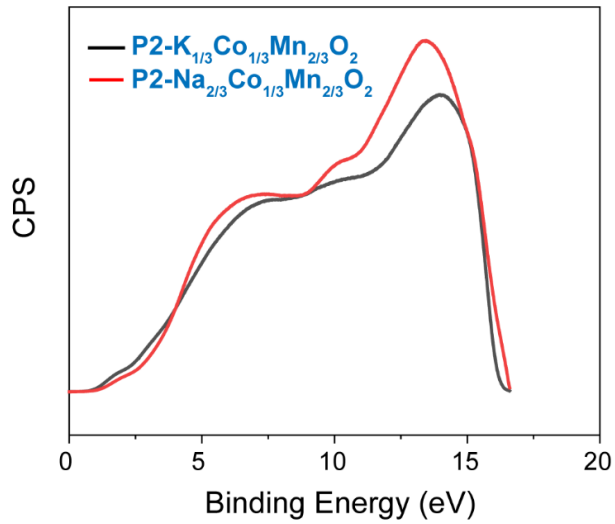

Figure S5. Comparative UPS spectra of the parent NCM and final KCM phases plotted with respect to the Fermi level.

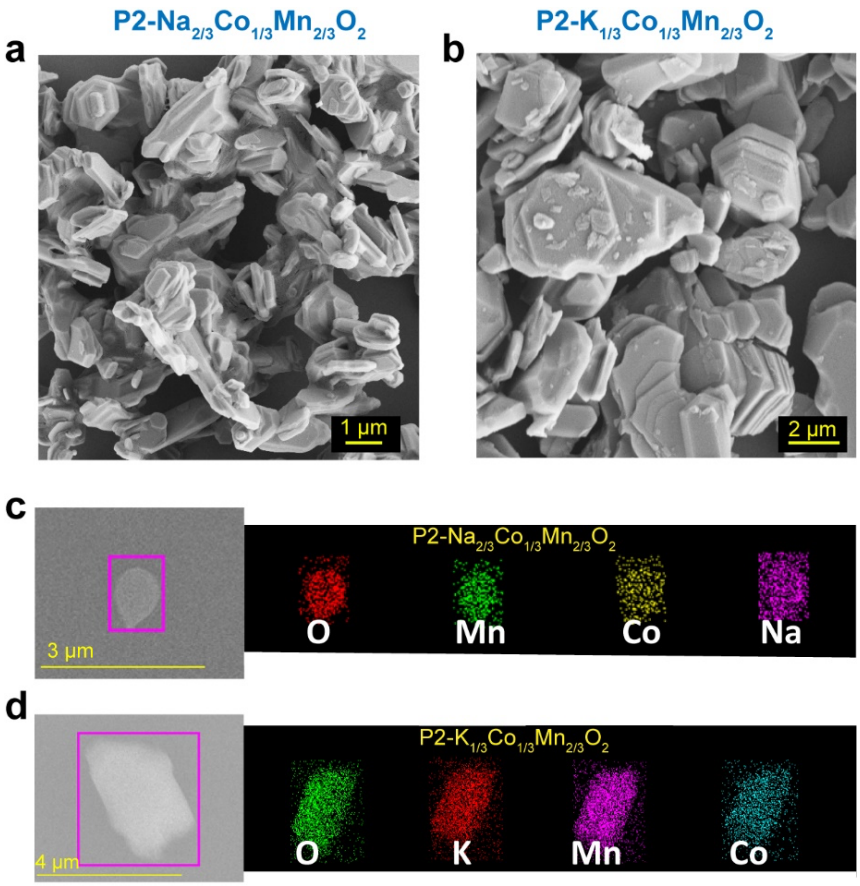

Figure S6. Morphology of (a) initial NCM and (b) final KCM compounds as revealed by scanning electron micrographs (SEM). SEM-EDS elemental mapping of parent P2-type $Na_{2/3}Co_{1/3}Mn_{2/3}O_2$ (top panel) and ion-exchanged P2-type $K_{1/3}Co_{1/3}Mn_{2/3}O_2$ (bottom panel).

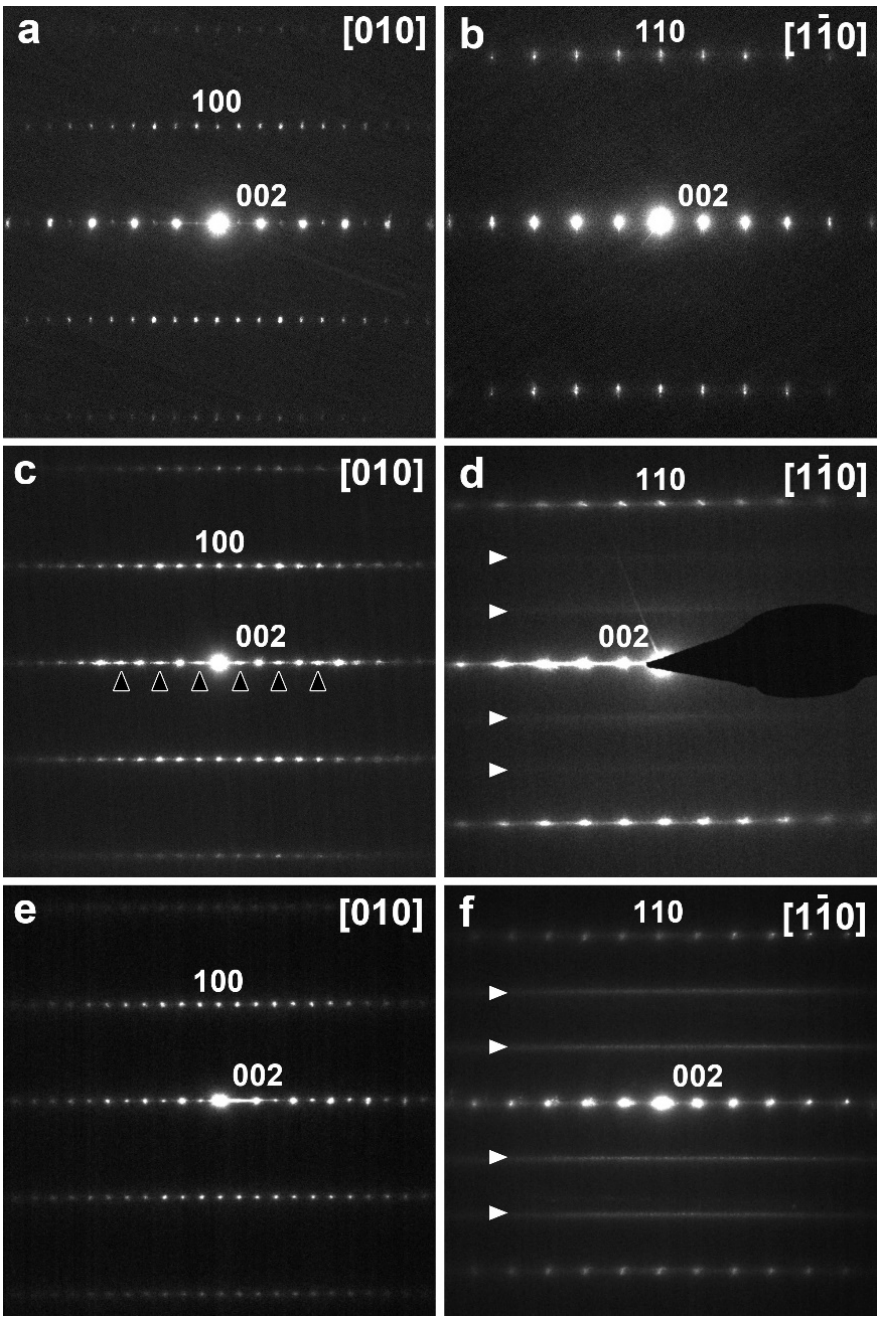

Figure S7. SAED patterns of the parent NCM phase (a, b), the intermediate phase formed after 3 h of cation exchange (c, d) and the target KCM phase (e, f). Black arrowheads mark diffuse 00*l*, $l \neq 2n$ reflections due to the alternating Na and K layer. White arrowheads mark diffuse intensity lines due to 2D ordering of K and vacancies within the alkali metal layers.

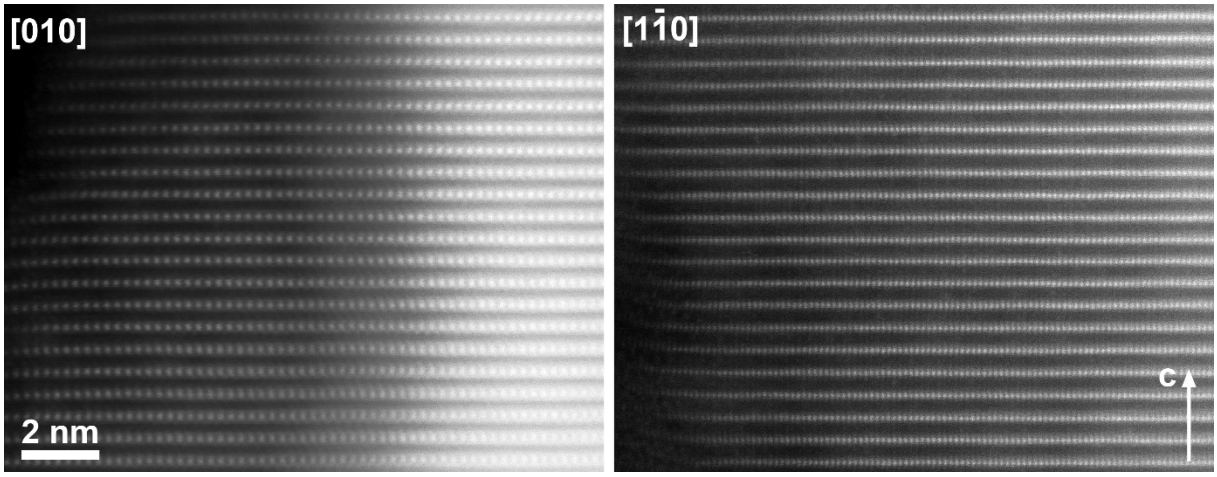

Figure S8. [010] and [1$\bar{1}$0] HAADF-STEM images of the parent NCM phase.

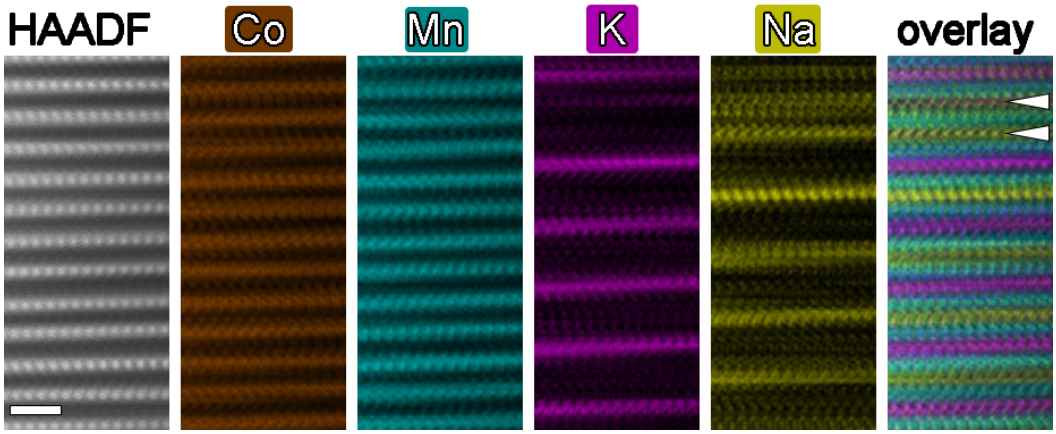

Figure S9. [010] HAADF-STEM image of NKCM and atomic resolution STEM-EDX maps demonstrating violation of alternating Na and K layers with occasional insertion of double Na layers (marked with arrowheads). The scale bar is equal to 1 nm.

Table S4. DFT (SCAN+*U*) calculated and experimentally observed lattice parameters for P2-type $K_xCo_{1/3}Mn_{2/3}O_2$ (x = 2/3,1/3 and 0).

		a (Å)	*b* (Å)	*c* (Å)	α (°)	β (°)	γ (°)	v(Å^3)
P2- $K_{2/3}Co_{1/3}Mn_{2/3}O_2$	SCAN+*U*	2.93	2.94	12.37	90.67	90.47	118.77	91.70
P2- $K_{1/3}Co_{1/3}Mn_{2/3}O_2$	SCAN+*U*	2.83	2.83	12.78	90.25	89.75	120.01	88.90
	Experiment	2.84	2.84	13.95	90.00	90.00	120.00	97.62
P2- $Co_{1/3}Mn_{2/3}O_2$	SCAN+*U*	2.84	2.84	10.12	90.04	89.98	119.96	70.84

Table S5. DFT (SCAN+*U*) calculated onsite magnetic moments of Mn and Co with the corresponding electronic configuration at different K-content in P2-type $K_xCo_{1/3}Mn_{2/3}O_2$ compositions.

Transition Metal	**P2-$K_{2/3}Co_{1/3}Mn_{2/3}O_2$**	**P2-$K_{1/3}Co_{1/3}Mn_{2/3}O_2$**	**P2-$Co_{1/3}Mn_{2/3}O_2$**
Mn	3.03 (4^+) - $t_{2g}^3 e_g^0$ 3.80 (3+)-$t_{2g}^3 e_g^1$	2.98 (4^+) - $t_{2g}^3 e_g^0$	3.12 (4^+) - $t_{2g}^3 e_g^0$
Co	0.04 (3^+) - $t_{2g}^6 e_g^0$	0.06 (3^+) - $t_{2g}^6 e_g^0$	1.06 (4^+) - $t_{2g}^5 e_g^0$

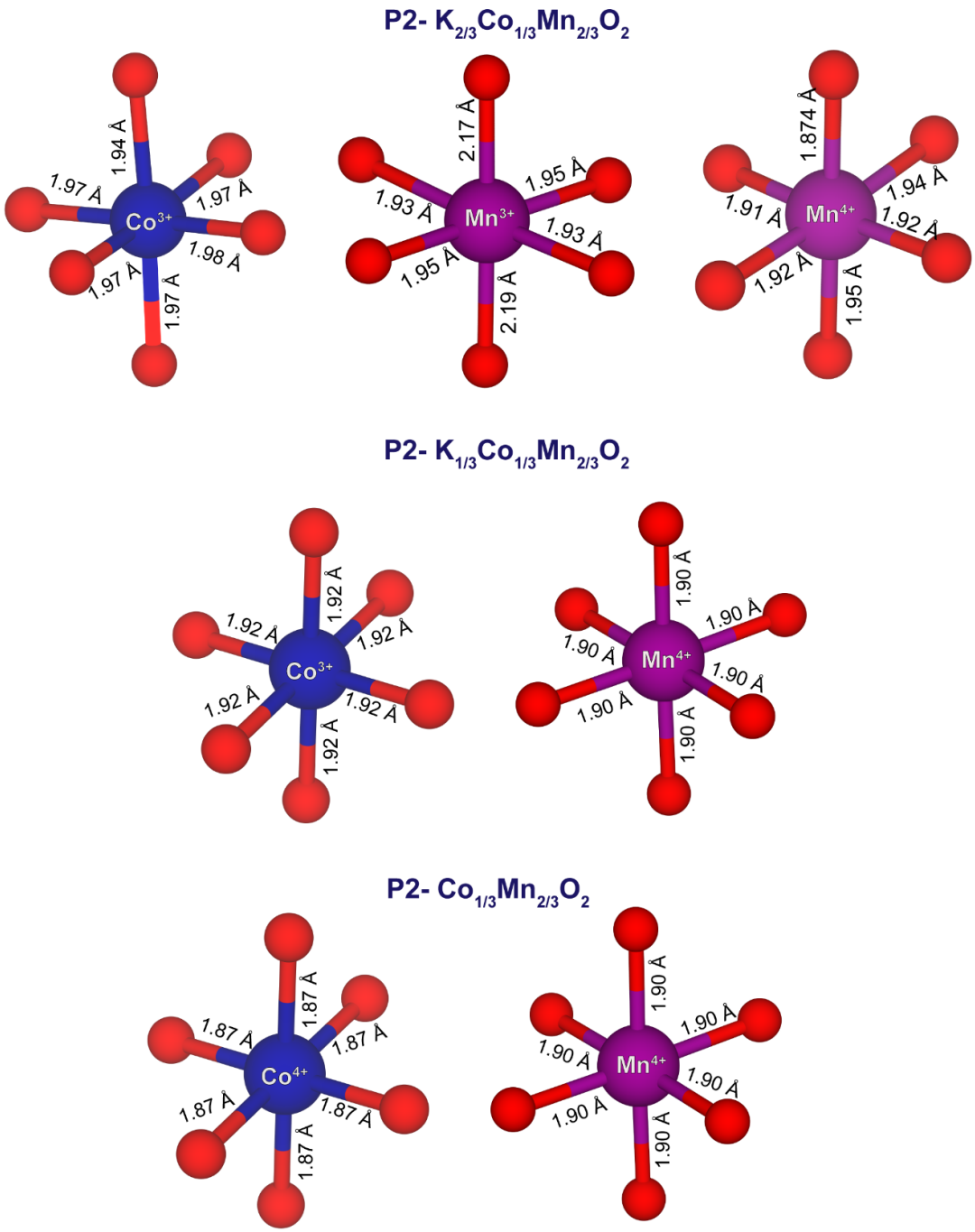

Figure S10. Bond lengths between Co–O and Mn–O in DFT (SCAN+*U*) calculated ground state structures for P2-type $K_xCo_{1/3}Mn_{2/3}O_2$ at different potassiated states (x = 2/3, 1/3, 0).

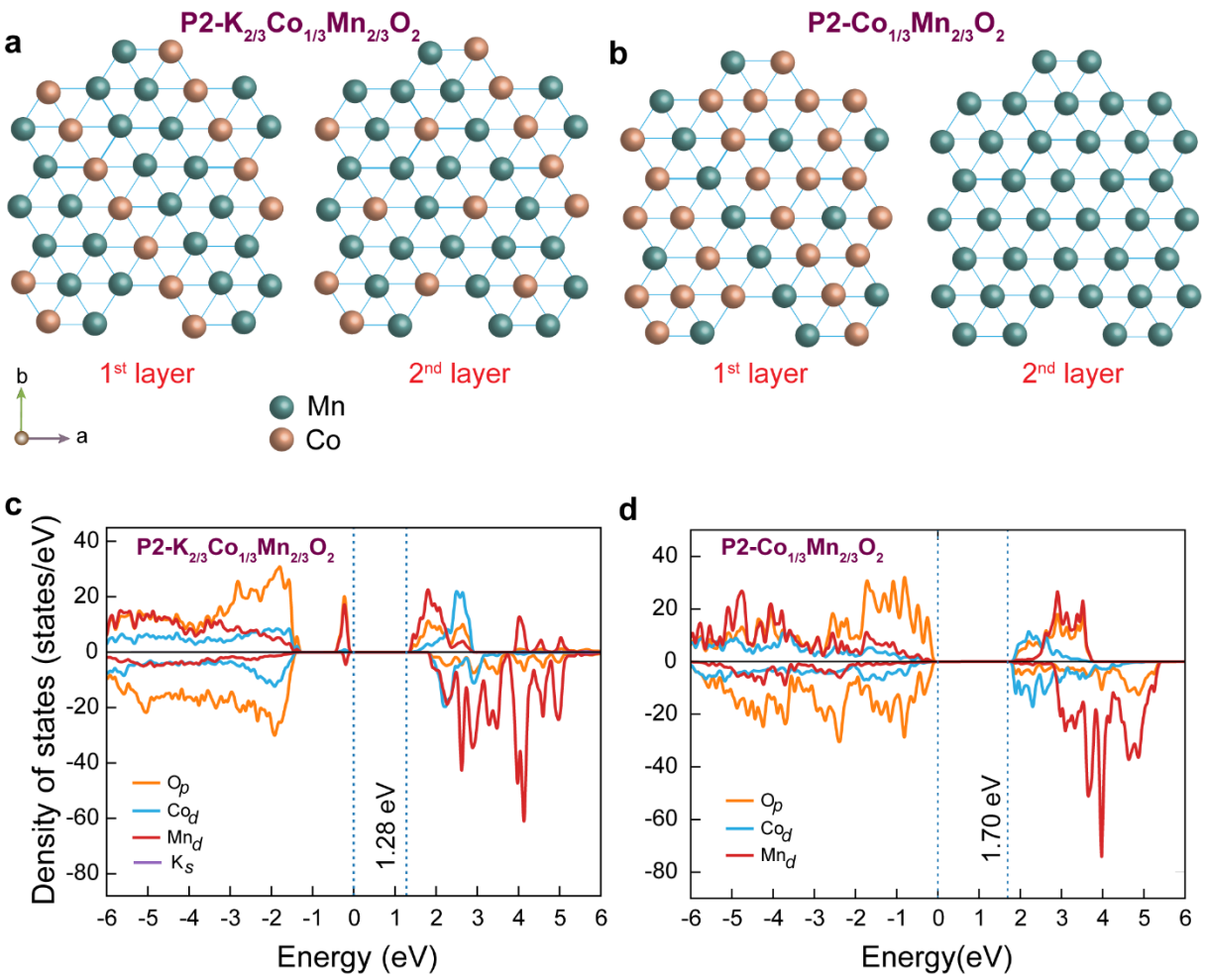

Figure S11. DFT (SCAN+*U*) calculated ground state in-plane preferential occupancy of Mn–Co in the basal transition metal (M) layer and adjacent (or top) M layer for (a) P2-type $K_{2/3}Co_{1/3}Mn_{2/3}O_2$ and (b) P2-type $Co_{1/3}Mn_{2/3}O_2$. (c-d) Corresponding projected density of states. Dotted blue lines denote the band edges, with the numerical values indicating the magnitutde of band gap.

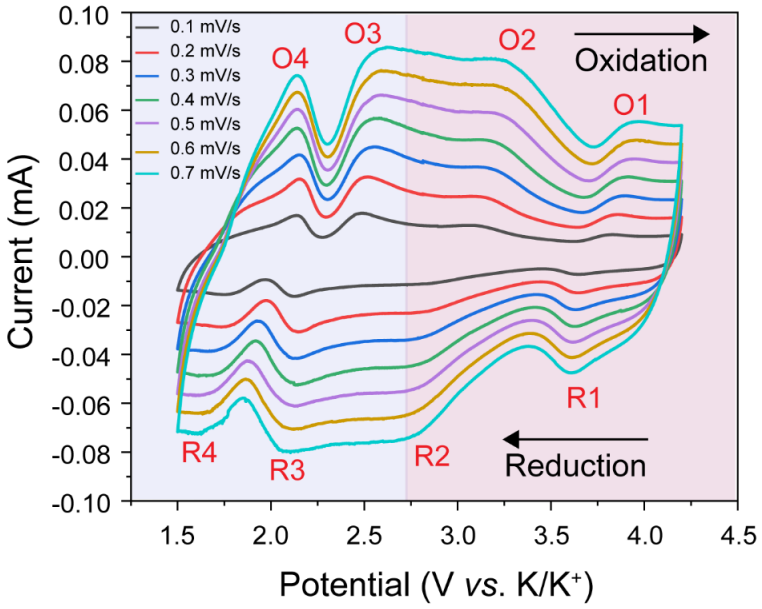

Figure S12. Cyclic voltammograms of the P2-type $K_{1/3}Co_{1/3}Mn_{2/3}O_2$ cathode at different scan rates.

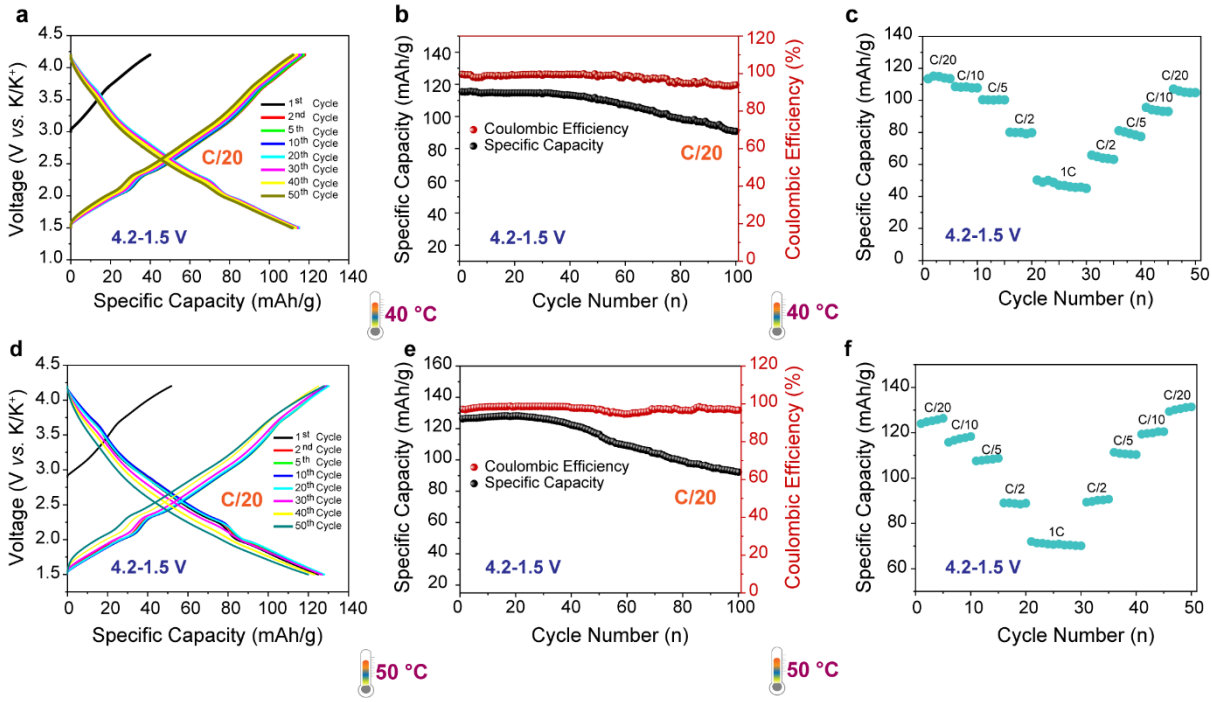

Figure S13. Electrochemical K^+ storage performance of P2-type $K_{1/3}Co_{1/3}Mn_{2/3}O_2$ cathode at 40° C (a-c) and 50° C (a and d). (a and d) Galvanostatic (dis)charge profiles (*vs* K/K^+). (b and e) Cycling stability curves at a current rate of C/20, and (e-f) cycling stability at different current rates.

Table S6. Lattice parameters of P2-type $K_{1/3}Co_{1/3}Mn_{2/3}O_2$ at different states of (dis)charge.

(Dis)charge State	*a* (Å)	*c* (Å)	Vol (Å^3)
Ch- 4.2V	2.83(7)	14.02(6)	97.76(6)
Dis- 3.5 V	2.84(2)	14.06(1)	98.36(5)
Dis- 3.2 V	2.84(4)	13.84(8)	96.99(9)
Dis- 2.0 V	2.85(3)	13.87(6)	97.82(7)
Dis- 1.5 V	2.85(1)	13.84(7)	97.39(6)

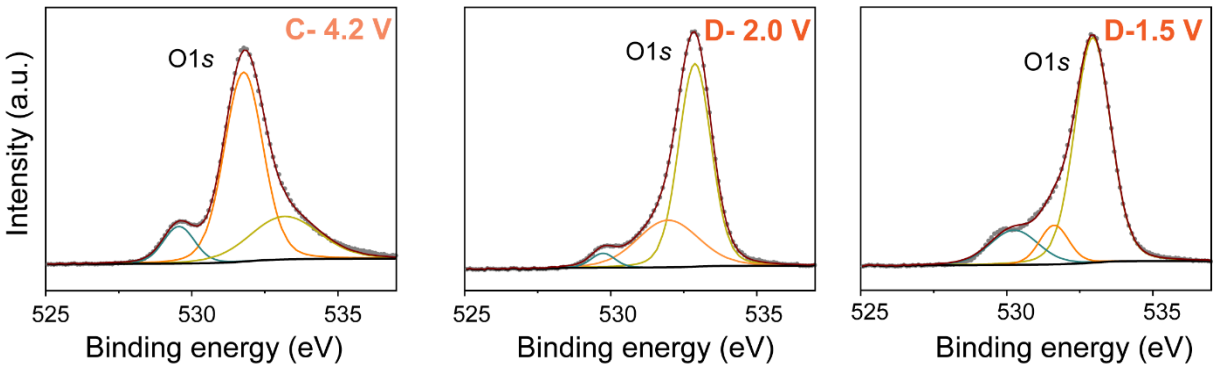

Figure S14. X-ray photoelectron spectroscopy (XPS) analysis of O 1*s* peak of KCM at different states of (de)potasssiation.

Table S7. XPS analysis of P2-type $K_{1/3}Co_{1/3}Mn_{2/3}O_2$ cathode at different states of (de)potasssiation. The oxidation states of Mn and Co species obtained from XPS analysis are closer to the DFT (SCAN+*U*) calculated values. Binding energies are given in eV.

Mn		Charge-4.2 V	Discharge-2.0 V	Discharge-1.5 V
Mn-2$p_{3/2}$ (FWHM-1 eV)	4+	641.01 641.84 642.69 643.60 644.61	--	--
Mn-2$p_{3/2}$ (f.w.h.m-1eV)	3+	--	640.53 641.60 642.46 643.47 644.70	--
Mn-2$p_{3/2}$ (f.w.h.m-1eV)	2+	--	--	640.79 641.82 642.69 643.57 644.56 645.63^{sat}

Co		Charge- 4.2 V	Discharge-2.0 V	Discharge- 1.5 V
Co-2$p_{3/2}$ (eV)	4+	779.98 781.19 782.89 789.70 ^{sat} (f.w.h.m-3.1 eV)	--	--
Co-2$p_{3/2}$ (eV)	3+	--	780.38 781.82 783.99 790.30 (f.w.h.m-1.68 eV)	780.27 781.48 783.35 790.19 (f.w.h.m-1.51 eV)

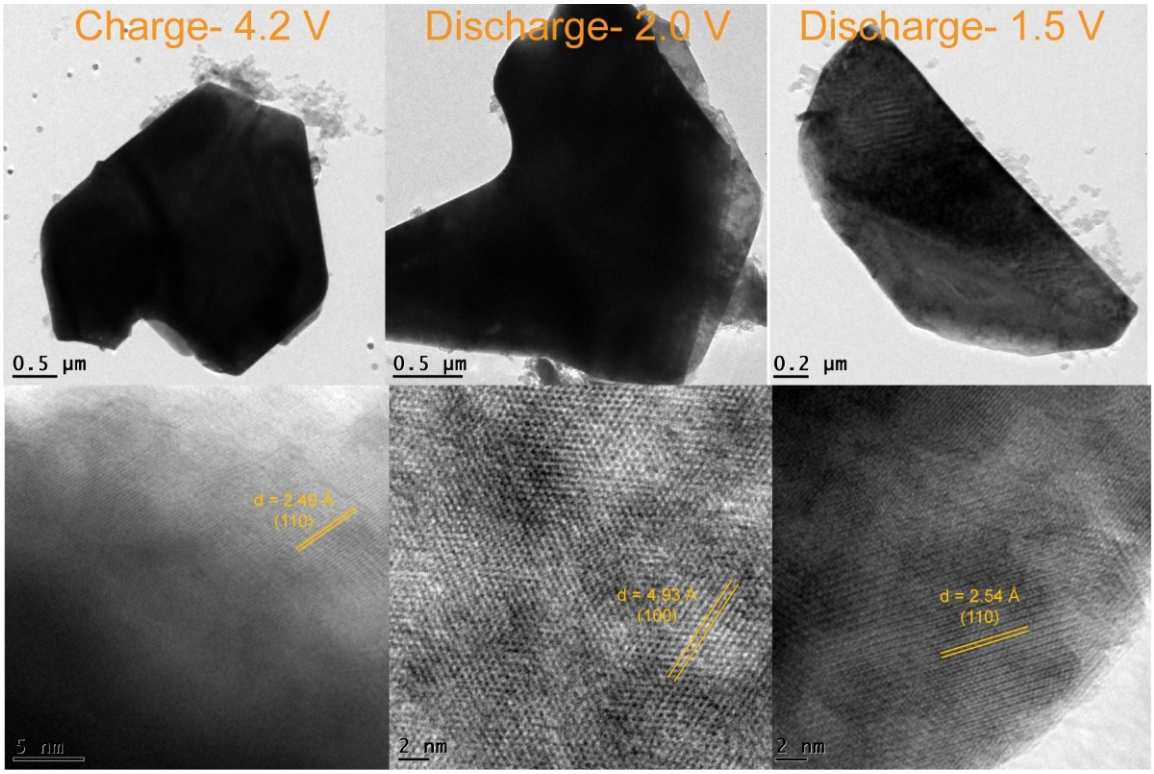

Figure S15. HR-TEM study showing the ex situ TEM images and corresponding lattice fringes of the P2-type $K_{1/3}Co_{1/3}Mn_{2/3}O_2$ cathode at different states of (dis)charge.